Constraining Earth's Core Composition from Inner Core Nucleation.

Alfred J. Wilson[1], Christopher J. Davies[1], Andrew M. Walker2, Dario Alfè[3,4,5]

[1]School of Earth and Environment, University of Leeds, Leeds, UK, LS2 9JT; [2]Department of Earth Sciences, University of Oxford, Oxford, UK, OX1 2JD; [3]Department of Earth Sciences, University College London, London, UK, WC1E 6BT; [4]University College London, London Centre for Nanotechnology, Thomas Young Centre, London, UK, WC1H 0AH; [5]Universita‘ di Napoli “Federico II”m Dipartimento di Fisica “Ettore Pancini”, Napoli, Italy, 80126
Email: a.j.wilson1@leeds.ac.uk

This manuscript will be submitted to Nature Communications.

Constraining Earth's core composition from inner core nucleation

Alfred J. Wilson[1*], Christopher J. Davies[1], Andrew M. Walker[2], Dario Alfè[3,4,5]

[1*]School of Earth and Environment, University of Leeds, Leeds, 100190, State, United Kingdom.
[2]Department of Earth Sciences, Organization, Oxford, OX1 2JD, United Kingdom.
[3]Department of Earth Sciences, University College London, London, WC1E 6BT, United Kingdom.
[4]London Centre for Nanotechnology, University College London, Thomas Young Centre, London, WC1H 0AH, United Kingdom.
[5]Dipartimento di Fisica "Ettore Pancini", Universita' di Napoli "Federico II"m, Napoli, 80126, Italy.

*Corresponding author(s). E-mail(s): a.j.wilson1@leeds.ac.uk;

Abstract

The composition of Earth's core is a fundamental property of the Earth's deep interior, defining its present structure and long term thermal and magnetic evolution. However, the composition of the core is not well understood, with several combinations of light elements being able to satisfy the traditional constraints from cosmochemistry, core formation and seismology. The traditional view of inner core formation does not include the necessity for liquids to be supercooled to below their melting point before freezing.

Attempts to calculate the magnitude of this supercooling have found that several simple core compositions are incompatible with inner core nucleation. Through molecular dynamics simulations, we show that nucleation from an $Fe_{1-x}C_{x=0.1-0.15}$ composition is compatible with a range of geophysical constraints. Whilst not a complete description of core chemistry, our results

demonstrate that inner core nucleation places strong constrain on the composition of Earth's core that may allow discrimination between previously identified potential compositions.

Keywords: inner core, nucleation, carbon

1 Introduction

The composition of Earth's iron rich core plays a crucial role in determining the structure, dynamics and evolution of Earth's deep interior. The melting temperature T_m of the core, set by the constituent iron alloy, defines the temperature T at the inner core boundary (ICB), which provides a unique constraint on the present-day temperature at the core mantle boundary [1] (CMB). Transport properties also vary with composition, including thermal conductivity k which controls the rate of secular cooling and therefore the long term thermal evolution of the core [1–3] and its potential to generate the global magnetic field, which has been preserved in the rock record for at least the past 3.5 Gyrs [4–6]. Light elements determine the strength of compositional buoyancy produced by inner core growth, the dominant power source for the geodynamo today [1, 7, 8], through their partitioning between solid and liquid during inner core freezing [9], while chemical exchange at the CMB may produce stable regions at the top of the core [10–12], that are detectable by seismology [13–15]. However, despite recent progress [16], the composition of the Earth's core remains poorly know.

Three main approaches have been used to constrain the composition of Earth's core: cosmochemistry, core formation and seismology. Core composition can be inferred via cosmochemistry by comparing the composition of primitive CI meteorites, those which most closely resemble the solar photosphere, with the silicate Earth. CI meteorites are rich in Fe, Ni, Mg, Ca, Al, Si, S, C and O [17], where the light elements Si, S, C and O are appealing candidates to explain the low density of the core compared to pure Fe [18]. If the Earth is assumed to be assembled primarily from

CI meteorites, deviations of the bulk silicate Earth from their composition can be ascribed to losses to space or the core. This approach favours an Fe-Ni (∼85 wt% and ∼5 wt%, respectively) [19] core where Si is the major light element (up to 9.6 wt% [20]) and C, S, and P cumulatively occupy 2.5 wt% of the core [19]. Core formation models estimate core composition by assuming chemical equilibrium between metal and silicate during Earth's accretion and differentiation. The equilibrium concentration of light elements depends on partition coefficients, determined by experiments and calculations, which vary with pressure, temperature and composition. The accretionary history of the Earth is therefore a key component in the determination of core composition. Several models [21–23] favour high Si and O (7.1-9.9 wt% and 1.3-5.3 wt% respectively) in the core. However, the array of accretionary histories which are possible result in a result in wide range of plausible compositions [24]. Comparison of the elastic properties of the core from seismology with results from mineral physics can be used to identify core compositions which are compatible with observations. The depth varying wave speeds of the outer and inner core and the density contrast across the ICB [25] require ternary systems but find that several combinations and concentrations of C, O, Si and S are viable [16]. For example, Badro et al. [26] find that whilst an Fe-Ni core with 3.7 wt% O and 1.9 wt% Si best satisfies the available constraints, other combinations of O with C, Si or S can also produce viable compositions. Ultimately, no single composition is uniquely able to explain the origins, formation and elastic properties of the Earth's core and the range of compositions which are plausible have markedly different implications for the thermal state of the core, both past and present. Given these uncertainties it is important to seek new constraints on core composition that are independent from but complementary to existing approaches. Here we propose that a constraint on core composition can be derived by analysing the thermodynamic conditions under which the solid inner core first formed.

The Earth's inner core is classically understood to have formed when the T of the core at the centre of the Earth cooled to the T_m at the same location. The composition of the core from this time onwards can be used to estimate the thermal profile of the deep Earth by assuming that the adiabatic temperature T_a of the core must equal the T_m at the inner core boundary [27] (ICB). However, this picture is physically incomplete because all liquids must be supercooled by an amount δT below T_m ($\delta T = T_m - T$), often significantly, before freezing can begin [28]. This requirement arises because whilst the solid phase is thermodynamically favoured for $T < T_m$, establishing an interface between solid and liquid is always unfavourable, and for the first solids the energy change of introducing an interface always wins out over the phase change. Previous studies [29–33] have estimated the δT required to nucleate the solid inner core for several compositions, that are otherwise broadly compatible with traditional constraints from core formation and seismology, but found that δT is incompatible with geophysical constraints (see Ref[34] for a review). Compositions including O and C were found to require δT far closer to geophysically compatible values when compared to pure Fe, Fe-S and Fe-Si [33]. Because not all potential compositions of the core can explain the presence of the inner core, inner core nucleation may provide a new and strong constraint on the composition of the core.

In this study we explore the Fe-C system further, for which the required δT for inner core nucleation is the closest to geophysical constraints of all systems tested previously[33]. We use molecular dynamic simulations to quantify the required conditions for nucleation in supercooled $Fe_{(1\text{-}x)}C_x$ liquids in the core. Our calculations address homogeneous nucleation where solids form spontaneously, away from any pre-existing solid surfaces. We return to consider heterogeneous nucleation, which arises in the presence of solid surfaces, in the discussion.

2 Results

We use classical molecular dynamics (CMD) to observe and characterise the nucleation of atomic-scale solids in supercooled $Fe_{(1-x)}C_x$ liquids at core pressures. Classical nucleation theory (CNT) [28] states that the nucleation rate I, inverse to the waiting time to observe nucleation τ_w, of a system increases with supercooling below the melting temperature.

2.1 Melting temperatures

To characterise nucleation in molecular dynamic simulations for a specific δT, we require knowledge of the melting temperature in order to define an appropriate simulation T. Liquidus temperatures (T_m) are calculated using two-phase coexistence simulations for compositions between $Fe_{0.98}C_{0.02}$ and $Fe_{0.9}C_{0.1}$, shown in Fig.1. Simulations are conducted at a range of T, volume (v) conditions, spanning the pressure (P) range of the inner core (330 - 360 GPa). At low P and x^C, T_m is comparable to the pure Fe case of Alfè, 2002 [35], the EAM of which is used for the Fe component of the model used in this study. At high P and low carbon concentration x^C, T_m depression is smaller than $Fe_{1-x}O_x$ of the same x (albeit at slightly lower P). T_m is depressed by a greater amount at high x^C, ∼1300 K at $x^C = 0.1$ and 330 GPa. Interpolation of results provides melting temperatures at 360 GPa, shown in Table 1.

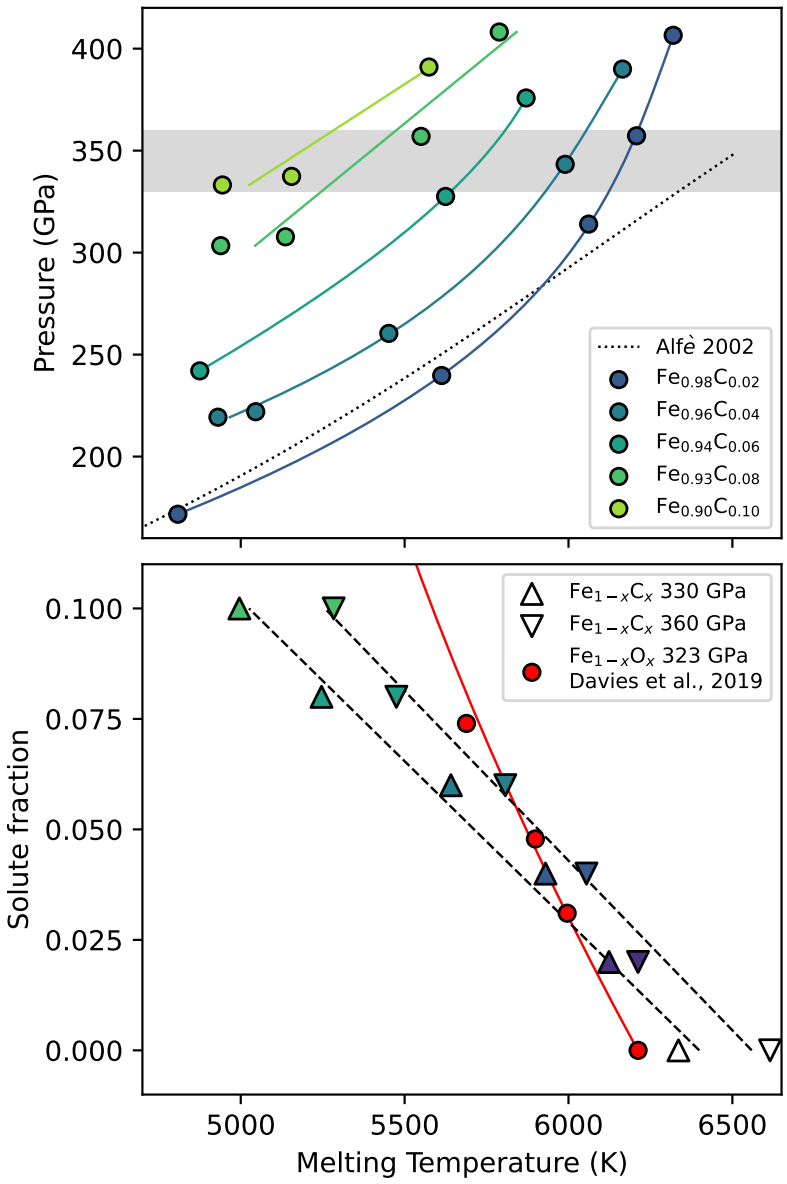

Fig. 1 Upper: Melting temperatures (points) calculated using two-phase coexistence simulations of $Fe_{1-x}C_x$ systems. Dotted line shows the melting curve of pure Fe from Alfè, 2002 [35] for reference. Solid lines are fits to data (2nd degree polynomial for $x^C = 0.02$, 0.04, 0.06 and linear for $x^C = 0.08$, 0.10). Grey shaded region shows the P range of the Earth's inner core. Lower: Interpolation of points in upper panel gives T_m(330 GPa,x^C) and T_m(360 GPa,x^C), shown as up and down pointing triangles, respectively. These conditions represent the present day ICB and centre of Earth, respectively. The $Fe_{1-x}O_x$ result of Davies et al., 2019 [30] at 323 GPa is shown for comparison (red points and line).

2.2 Nucleation of iron-carbon alloys

We use CMD simulations of supercooled iron alloys to study the nucleation of solids. These simulations are independent of CNT; however, CNT provides an intuitive physical picture with which to interpret the simulation results. From our simulations we obtain $I(r)$ directly for sub-critical nuclei and using CNT we are then able to fit for the critical nucleus size r_c, which has a 50% chance of spontaneously freezing a system, which informs the average waiting time τ_w to observe the freezing of a system (see methods). This approach means that systems with low supercooling, and therefore small $I(r_c)$ and large τ_w, can be studied directly, avoiding large extrapolation necessary in prior approaches [30].

Critical radii r_c are estimated from $I(r)$ recorded from CMD simulations (see methods and Wilson et al., 2021 [31] for details) at selected T and x^C and are shown in Fig. 2 with comparison to prior results for $x^C = 0.01$ and $x^C = 0.03$ from Wilson et al., 2023 [33]. $\tau_w = \tau_0 \exp\left(\frac{\Delta G(r_c)}{k_B T}\right)$, where $\Delta G = \frac{4}{3}\pi r^3 g^{sl} + 4\pi r^2 \gamma$, g^{sl} is the free-energy difference between solid and liquid phases, γ is the interfacial energy at the boundary between solid and liquid, k_B is the Boltzmann constant and τ_0 is a kinetic prefactor ($\tau_0 = \frac{z}{NS}$) linked to the probability of freezing or growing a nuclei z, the number density of nucleation sites N and the growth rate of nuclei S (all of which are calculated from simulations). The remaining quantities required to calculate τ_w (h_f, h_c and γ) are fit from $r_c(T) = \frac{-2\gamma}{h_f \frac{\delta T}{T_m}(1-h_c \delta T)}$, at each x^C (Fig. 2, see methods for details).

The interatomic potential developed here reproduces the r_c result of Wilson et al,. 2023 [33] at $x^C = 0.01$ and 5000 K within 4% ($r_c = 9.16 \pm 1.86$ Å compared to $r_c = 9.52 \pm 2.31$ Å[33]). At all tested values of δT, increasing x^C reduces r_c although at large δT r_c for all compositions are within uncertainty of one another. Simulations with $x^C > 0.1$ proved unstable making tests at greater x^C impossible for the EAM developed here.

	Wilson et al., 2023		This study	
	$Fe_{0.99}C_{0.01}$	$Fe_{0.97}C_{0.03}$	$Fe_{0.95}C_{0.05}$	$Fe_{0.90}C_{0.10}$
N (m^{-3})	6.8×10^{-35}		2.3×10^{-34}	2.8×10^{-34}
S (s^{-1})	5×10^{13}		1.2×10^{12}	1.6×10^{12}
τ_0 (s m^{-3})	2.93×10^{-23}	4.63×10^{-23}	6.48×10^{-23}	1.51×10^{-22}
h_f (J m^{-3})	0.57×10^{10}	1.30×10^{10}	$1.35\times10^{10} \pm 2\times10^{9}$	$1.55\times10^{10} \pm 2.5\times10^{9}$
h_c	1×10^{-3}	1×10^{-6}	$1\times10^{-6} \pm 5\times10^{-7}$	$1\times10^{-6} \pm 5\times10^{-7}$
γ (J m^{-2})	1.005	1.005	1.005 ± 0.01	1.005 ± 0.004

Table 1

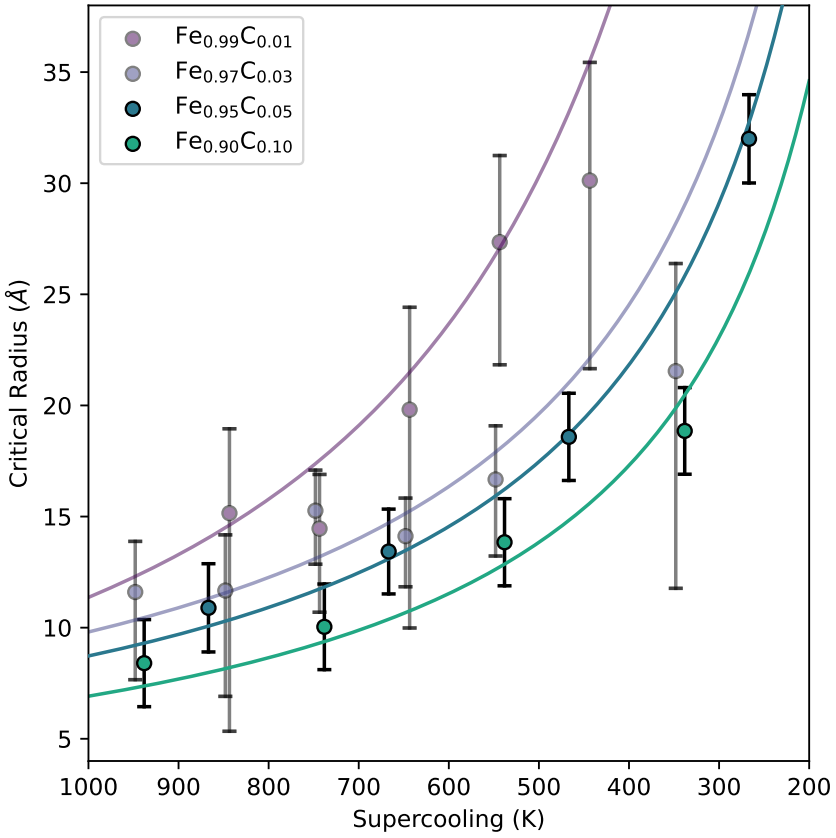

Fig. 2 Critical radii for liquid $Fe_{1-x}C_x$ alloys between $x^C = 0.01$ and $x^C = 0.1$ ($x^C = 0.01$ and $x^C = 0.03$ cases are taken from Wilson et al., 2023 [33]) all at 360 GPa. r_c is estimated from distributions of sub-critical nuclei. Temperature is shown as supercooling ($\delta T = T_m - T$, where T_m is unique for each x^C Fig.1).

Values of τ_w are shown in Fig. 3. Results for $x^C = 0.01$ and 0.03 are from Wilson et al., 2023 [33], while results for $x^C = 0.05$ and 0.10 are calculated from the quantities

shown in Table 1. The number of nucleation sites (N) and rate of nuclei growth (S) are calculated as averages from nuclei distributions and allow calculation of τ_0 (see methods). τ_0 is not found to vary with supercooling by more than one order of magnitude and so is taken as isochemical averages. Estimates of τ_w are compared to the value 3.1 $\times 10^{34}$ s m^{-3}, which is a moderate waiting time the Earth's core might have sustained supercooling prior to inner core nucleation [33] (black dashed line, Fig. 3) and implies that a region with half of the present day inner core was supercooled for 1 Gyrs prior to nucleation. To produce a critical nucleation event in this waiting time, the $x^C = 0.05$ and $x^C = 0.1$ cases require $\delta T = 580^{+97}_{-71}$ K and $\delta T = 481^{+95}_{-67}$ K, respectively.

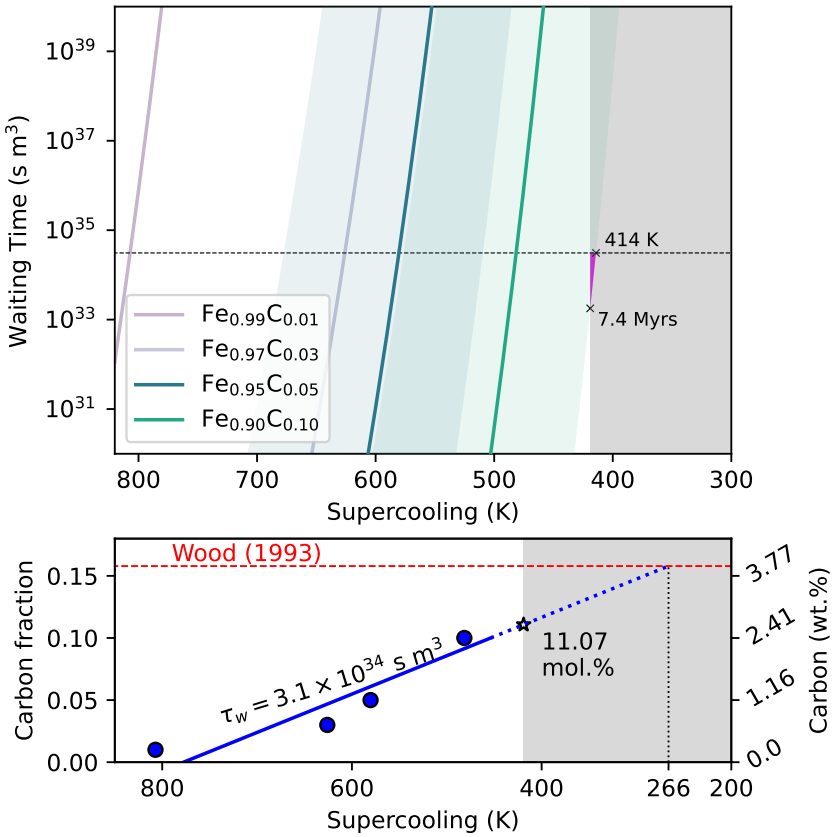

Fig. 3 Upper: Waiting time for a critical nucleation event to occur for four $Fe_{1-x}C_x$ compositions at a range of supercooling. Uncertainties are shown for the predictions of this study (x^C = 0.05 and x^C = 0.1) as shaded colours. Estimates from Wilson et al., 2023 [33] for x^C = 0.01 and x^C = 0.03 are also shown (without uncertainty for clarity). The dashed black line shows the maximum waiting time for an inner core half its present radius supercooled for 1 Gyr and the grey shaded region represents supercooling values compatible with the present day size of the inner core [33]. The pink area highlights areas of the $Fe_{0.9}C_{0.1}$ uncertainty envelop which represent a geophysically compatible supercooling [33] Lower: Interpolation (solid blue line) and extrapolation (dashed blue line) of $Fe_{1-x}C_x$ results (solid lines, without exploring uncertainty) at $\tau_w = 3.1 \times 10^{34}$ s m^3 to estimate the δT needed to nucleate the inner core for values of x^C up to the maximum proposed C content of the core, $x^C = 0.156$ (red line) [36].

3 Discussion

Our results for a carbon concentration of $x^C = 0.1$ do, strictly, represent a route to homogeneously nucleating solids at the centre of the completely liquid core because the allowable supercooling of the core and the required supercooling for nucleation

match within uncertainty (fig. 3). However, the value of 420 K for the allowable supercooling is a maximum obtained by considering many different published melting curves and core temperature profiles [33]. It is therefore of interest to understand how the required supercooling can be further reduced below this value, which can be achieved for larger values of x^C.

The EAM developed in this study and used to define molecular dynamic simulations which characterise nucleation behaviour of $Fe_{1\text{-}x}C_x$ alloys cannot be used for x^C above 0.1 (see Methods). We therefore extrapolate our results at lower x^C (lower panel, Fig. 3) to predict how the supercooling requirement to spontaneously freeze the Earth's inner core might change with higher x^C. Previous studies suggest that up to 15.2 mol% (4 wt.%) C might have entered Earth's core following accretion [36]. If extrapolated linearly to this concentration, given a waiting time of 3.1×10^{34} s m^3, inner core nucleation requires only 266 K of supercooling.

The melting temperature T_m at ICB conditions for a liquid carbon concentration $x^C = 0.1$ is around 5000 K (fig. 1). This value is lower than the range 5300-5900 K obtained by previous studies for the Fe-O system with O concentrations in the range 8-17 mol% [37], though it is comparable to estimates of T_m when H is a primary light element in the core [38]. The corresponding CMB temperature, estimated by projecting an adiabat from the ICB temperature using values from the Preliminary Reference Earth Model [25] and a Grüneisen parameter in the range 1-1.5 [39] is $\sim$3500 K, which is below estimates of the lower mantle solidus [40, 41] as required by the observed absence of pervasive melt in the lower mantle.

Until now we have assumed that the inner core nucleated homogeneously. Heterogeneous nucleation offers an alternate route to inner core formation but requires identification of a pre-existing solid surface to act as a nucleation site. Whilst nucleation in nature typically occurs in the presence of such surfaces, this still requires supercooling. In heterogeneous nucleation the free-energy of homogeneous nucleation

ΔG (see methods) is reduced due to a smaller solid-liquid interface being established compared to the homogeneous case (see Wilson et al. [34] for a review). The wetting angle between the nucleating metallic phase and the pre-existing solid controls the surface contact between the two solid phases and therefore defines the energetic benefit of heterogeneous nucleation compared to the homogeneous case.

One candidate heterogeneous nucleation site is oxides originating from the CMB, for example precipitates from the cooling liquid core [42, 43]. Previously considered oxides (FeO, MgO, SiO_2) [29, 34] do not possess the key criteria for viability: sufficient density to be able to reach the centre of the Earth where the core is first and most supercooled and low solubility and high melting temperature in order to avoid dissolution or melting and remain solid in the core[34]. Even with these characteristics, the wetting angle between metals and oxides at 1 bar ranges from 110-180 degrees which corresponds to a reduction of at most 200 K for pure Fe in the Earth's core [29]. The resulting δT remains geophysically incompatible, meaning that a system with smaller δT for homogeneous nucleation is needed for a viable heterogeneous mechanism.

Metallic phases [29] typically have higher density and wetting angle compared to oxides. Identifying a phase which avoids dissolution and melting in liquid iron remains a challenge and metals considered thus far are unlikely to reach Earth's centre [29, 34]. At present there is no material known to possess the required attributes to act as a site for heterogeneous inner core nucleation, and no geophysical scenario to explain how this material was delivered to the core. In the event that such a solid is discovered and required for inner core nucleation the pre-existing solid itself will place constraint on the bulk core composition, as will the nucleating phase.

The composition of Earth's core is likely to be more complex than the simple binary alloys we have considered [44, 45]; however, it is nevertheless useful to discuss our simplified Fe-C compositions in the context of the available constraints. Geophysical constraints employ the radially-varying core density and seismic wavespeeds. C and

O partition strongly into liquid iron on freezing [44, 46] and are currently the primary candidates to explain the density jump $\delta\rho$ at the ICB. The C concentrations we consider are compatible with the values of the $\delta\rho$ = 0.6-1.0 gm cm^{-3} derived from seismic normal modes [47], though plausible O concentrations can also explain the $\delta\rho$ observations. Matching the core mass as well as $\delta\rho$ requires at least one other light element that partitions more evenly between inner and outer core, e.g. S or Si [44] or H [48]. Ab initio calculations [38] indicate that Fe-C alloys with $>$ 15 mol% C, compatible with the geophysically allowable supercooling of the core, can match the seismically observed CMB and ICB density as well as the CMB P-wave velocity; however, the predicted ICB P-wave velocity is higher than observed. In the inner core, the anomalously high compressional/shear wave velocity is thought to relate to the presence of small amounts of O or C [16]. Depletion of the bulk silicate Earth compared to CI chondrites suggests that up to 15 mol% C could be in the core [36]. Recent experimental determinations of C partitioning between liquid iron alloys and silicate melts conducted in the pressure-temperature ranges 37-59 GPa and 4200-5200 K [49] and 49-71 GPa and 3600-4000 K [50] show that C becomes less siderophile as P and T increase, which when applied to a specific model of core formation indicate that C does not partition strongly into the core. However, these estimates depend strongly on mantle chemistry and the assumed core formation scenario, both of which are uncertain at present [16].

In summary, Fe-C binary alloys can satisfy some but not all constraints on the core composition. Studying nucleation is challenging even in binary alloys [30, 33] and to date no studies of ternary alloys have been attempted. Nucleation in the Fe-H system has also not been studied, though the weaker effect of H on the melting point [48] may suggest longer waiting times than we have found in the Fe-C system. Other light elements have been shown to stabilise phases of iron [51] which might nucleate more readily than those favoured in the core [32], however, this effect has

not been observed in binary systems so far [33]. Ultimately, while many candidate compositions are able to reproduce available constraints from cosmochemistry [36], core formation [52], seismology [38, 44, 46], only an Fe-C composition has so far been shown to explain the nucleation of the inner core. Hence, we argue that the process of inner core nucleation can provide a novel and strong constraint on core composition. It is therefore worthwhile to reconsider previous inferences of core composition in light of this new constraint.

The existence of a precipitated solid phase in the liquid core would present a route for heterogeneous nucleation of the inner core. However, the required δT for this mechanism will depend on the solid and the composition of the core. Our results have shown that only some compositions reduce δT. Therefore, a viable heterogeneous nucleation site, which avoids dissolution and melting, still places constraint on the core's composition. The amplitude of the energetic barrier to nucleation will be different for each precipitated solid phase in the core.

4 Conclusion

Inner core nucleation subject to a supercooling of 200-400 K has potentially significant implications for interpreting the structure, dynamics, and evolution of Earth's core. The predicted supercooling would delay the inner core formation age predicted by core evolution models by $O(100)$ Myrs [53, 54]. In classical evolution models with high core conductivity [55] this delay would likely imply a lack of power available to the dynamo prior to inner core formation, in conflict with paleomagnetic observations [56, 57]. This observation lends support to evolutionary scenarios that include long-lived dynamo power supplied by precipitation of oxides at the CMB [58–62], though the effect of C on the partitioning behaviour at the CMB has not been systematically evaluated and may influence the power provided by precipitation. Sudden rapid growth of the inner core following nucleation may leave a signature in the paleomagnetic record owing

to the additional latent heat and gravitational power to the dynamo [29], though the expected influence on field intensity and variability has not yet been studied in detail. Finally, delayed inner core formation may influence texturing of the inner core, for example by trapping liquids in the solid [53], and has been correlated with the existence of the innermost inner core [54].

5 Methods

5.1 Interatomic potential

We use classical molecular dynamic (CMD) simulations of liquid $Fe_{1-x}C_x$ to characterise nucleation behaviour at a range of T and x^C. To describe the interatomic forces and system energies in our simulations, we develop an embedded atom model (EAM) which is trained on ab initio calculations. The model is fit to reproduce the positions, energy (E) and P of snapshots from ab initio molecular dynamics (AIMD) calculations run using the VASP software package [63] with the projector augmented wave method [64] and the PW91 generalised gradient approximation functional [65]. Details of these calculations follow Wilson et al., 2023 [33] which shares some of the same AIMD data at low x^C used for fitting the potential. The EAM potential is validated against a separate suite of AIMB snapshots to ensure that E and P are accurately reproduced. The root mean square of fluctuations in E are determined to be 0.292 and 0.316 eV per cell at 5000 K for $Fe_{0.95}C_{0.05}$ and $Fe_{0.9}C_{0.1}$, respectively, far less than k_B/T (0.431 eV). Reproduction of liquid structure is confirmed by comparison of radial distribution functions where average positions of neighbouring atoms in CMD simulations are within 0.05 Å of AIMD simulations for all interactions and all v, T, x^C conditions.

AIMD simulations are performed by melting systems of 128 atoms with different carbon fractions (close to 20, 10 and 5 mol. %) at 10000 K for 1 ps before equilibrating at a target T (4000, 5000 and 6000 K) for 1 ps and evolving the system at the target

T for 30 ps. The simulation cell volume is tuned for each composition and target T to achieve a P of 360 GPa. From the final 30 ps of simulation time, configurations are selected at every 100 fs as data on which the EAM is trained. The total energy E of a $Fe_{1\text{-}x}C_x$ system is defined by the EAM as the sum over contributions from all atomic interactions

$$E = \sum_{i=1}^{N_{Fe}} E_i^{Fe} + \sum_{i=1}^{N_C} E_i^C + \sum_{i=1}^{N_{FeC}} E_i^{FeC}. \tag{1}$$

Each interaction, between atoms i and j, contains repulsive Q and embedded F contributions. Q depends on the interatomic distance r_{ij} which also defines an electron density ρ_{ij} on which F depends. E for each type of interaction is given by

$$\begin{aligned} E_i^{Fe} &= Q_i^{Fe} + F^{Fe}(\rho_i^{Fe}) \\ &= \sum_{j=1,j\neq i}^{N_{Fe}} \epsilon^{Fe} \left(a^{Fe}/r_{ij}\right)^{n^{Fe}} - \epsilon^{Fe}\dot{C}^{Fe}\sqrt{\rho_i^{Fe}}, \end{aligned} \tag{2}$$

$$\begin{aligned} E_i^{C} &= Q_i^{C} + F^{C}(\rho_i^{C}) \\ &= \sum_{j=1,j\neq i}^{N_{C}} \epsilon^{C} \left(a^{C}/r_{ij}\right)^{n^{C}} - \epsilon^{C}\dot{C}^{C}\sqrt{\rho_i^{C}}, \end{aligned} \tag{3}$$

$$\begin{aligned} E_i^{FeC} &= Q_i^{FeC} \\ &= \frac{1}{2}\sum_{i=1}^{N_{Fe}} \sum_{j=1,i\neq j}^{N_{C}} \epsilon^{FeC} \left(a^{FeC}/r_{ij}\right)^{n^{FeC}}, \end{aligned} \tag{4}$$

where the respective densities are

$$\rho_i^{Fe} = \sum_{j=1,j\neq i}^{N_{Fe}} \left(a^{Fe}/r_{ij}\right)^{m^{Fe}} + \rho_i^{FeC}, \tag{5}$$

$$\rho_i^{C} = \sum_{j=1,j\neq i}^{N_{C}} \left(a^{C}/r_{ij}\right)^{m^{C}} + \rho_i^{FeC}, \tag{6}$$

and

$$\rho_i^{FeC} = \sum_{j=1, j\neq i}^{N_C} \left(a^{FeC}/r_{ij}\right)^{m^{FeC}}. \quad (7)$$

Here, ϵ, a, n, m and $\dot{C}$ are free parameters to be fit for each interaction and are reported in Table 2. Simulations where $x^C > 0.1$ are found to dissociate into two

	ϵ	a	n	m	$\dot{C}$
Fe	0.166200 eV	3.471400 Å	5.930000	4.788000	16.550000
FeC	0.384726 eV	2.601660 Å	4.380769	4.933012	
C	0.019805 eV	2.311113 Å	9.532860	6.967342	13.880981

Table 2 Parameters for EAM model fit to FPMD data at several C concentrations and temperatures. Fe values, from Alfè, 2002 [35], are fixed during fitting.

components, Fe rich and C rich, and are discarded from our analysis. Given the expense our calculations (∼4 million CPU hours), developing an additional EAM for such conditions is not within the scope of this study.

5.2 Melting temperatures

The melting temperatures of $Fe_{1\text{-}x}C_x$ are calculated with coexistence simulations using the EAM potential and the LAMMPS simulation package [66]. Systems of 128000 atoms are arranged into a long periodic cell where the x axis is 3 times the length of y and z axes. All atoms are initially arranged in a hexagonally close packed structure with C atoms randomly replacing Fe atoms to achieve the desired concentration. The positions of atoms in the central 50% of the simulation are initially fixed in space whilst the other half is melted at 10000 K for 5 ps. This procedure establishes the two phase system. The entire system is then evolved at a target T under the NVT ensemble for 1 ps to establish the target average kinetic energy. Finally, the system is evolved for 10 ps under the NVE ensemble, allowing the solid region of the system to grow or melt. Once a system has reached equilibrium, the T will lie on the melting curve, meaning that the time averaged T and P provide a single T_m. The random distribution of C into the initial system provides many different initial x^C for the solid

and freezing and melting of the solid allows for C partitioning between the solid an the liquid. Systems with $x^C > 0.05$ in the solid see much of the solid melt before freezing a lower x^C solid. This process shows that whilst C cannot diffuse freely in the solid over the timescale of these simulations, systems tend towards chemical equilibrium through freezing and melting. Simulations which stabilise T and P have $k_D = 4 \pm 2$ (where $k_D = \frac{x^C_{liquid}}{x^C_{solid}}$) which is consistent with ab initio calculations [46]. We estimate the uncertainties of each $T_m(v, x)$ point from the fluctuations of T and P over the final 1 ps of simulation time and discard any simulations which entirely freeze, melt, or do not achieve equilibrium. Because of the constant volume and energy conditions, T and P are unknown prior to the simulation setup. In order to define $T_m(P, x)$ we explore a range of initial T and v and interpolate our results for T_m(360 GPa,x).

5.3 Nucleation theory

In this study we use classical nucleation theory (CNT) to describe the nucleation behaviour of CMD simulations of iron alloy liquids at the conditions of Earth's core. Previous studies [30–33] have consistently found that predictions from CNT are consistent with outputs from MD simulations, accurately describing the distribution of nucleus sizes and the dependence of nucleation rate on supercooling. We note that our CMD simulations are completely independent of CNT; indeed, these simulations have been used to show that non-classical effects such pressure waves have no effect on the nucleation of solids in Earth's core [30]. According to CNT, the requirement for liquids to be supercooled prior to freezing via homogeneous nucleation arises from a competition between two energetic contributions to the total free energy (ΔG) associated with forming a solid nucleus in a supercooled liquid. The first contribution is the free energy release (g^{sl}) associated with transforming supercooled liquid into a solid, which is always favourable when below the melting temperature and occurs through random fluctuations in the liquid producing "solid-like" configurations of atoms. The

second contribution (γ) is associated with forming an interface between the liquid and solid and is always unfavourable. These two components are scaled by the volume and surface area of the newly formed nucleus of radius r to define a total free-energy change on formation

$$\Delta G(r) = \frac{4}{3}\pi r^3 g^{sl} + 4\pi r^2 \gamma \tag{8}$$

for spherical particles.

The rate I at which a nucleus of radius r forms is defined by Boltzmann statistics:

$$I(r) = I_0 \exp\left(\frac{-\Delta G(r)}{k_B T}\right), \tag{9}$$

where k_B is Boltzmann's constant and I_0 scales the nucleation rate of the specific system. Eq. 9 shows that small nuclei are likely to form often (or equivalently, require less waiting time ($\tau_w \approx I^{-1}$) before they occur); however, Eq. 8 shows that these nuclei will remelt rather than grow because of the large influence of surface area on the free energy at small r. Despite a low probability, continued growth is possible given a sufficiently long waiting time and large system volume to observe random fluctuations which produce a larger nucleus. Above a critical radius $r_c = -2\gamma/g^{sl}$ at the peak of ΔG the volume term in Eq. 8 increases with radius faster than surface term, meaning that whilst still having an overall unfavourable free energy for forming a nucleus, continued growth is thermodynamically favoured when compared to remelting. Greater supercooling requires a smaller r_c in order to freeze a system, which in turn requires less waiting time for the critical event to spontaneously occur.

The rate at which a nucleus of size r spontaneously forms in a supercooled liquid is given by Eq. 9. When framed in terms of r_c the inverse of nucleation rate describes the average duration before a supercooled system will experience a critical nucleation event and freeze

$$\tau_w = \tau_0 \exp\left(\frac{\Delta G(r_c)}{k_B T}\right), \tag{10}$$

where

$$r_c = \frac{-2\gamma}{g^{sl}}. \tag{11}$$

The prefactor τ_0 can be described by

$$\tau_0 = \frac{z}{NS}, \tag{12}$$

where the Zeldovich factor z is related to g^{sl} through

$$z = \left(\frac{\frac{4}{3}\pi r_c^3 g^{sl}}{k_B T} \right)^{-1/2}. \tag{13}$$

and, N and S are the number of available nucleation sites and the rate of nuclei growth, respectively. To quantify N, S and $I(r)$ solid-like arrangements of atoms are identified at each timestep in the same manner as our previous studies [31, 33] following Rein et al., 1996 [67]. Therefore, all quantities required to calculate τ_w are accessible via CMD calculations. Because r_c is predicted to be large for the P and T of the early Earth's supercooled liquid core [31], simulations at >4000 K and 360 GPa cannot be expected to produce a nucleus of the critical size (>30 Å). Instead, r_c is predicted by recording the rate at which smaller nuclei (which are more common) are observed in simulations, informing $I_T(r)$ where r is small. At a fixed T all quantities in Eq. 8 are constant so we can write

$$-\ln\left(I_T(r)\right) \propto \Delta G_T(r) \tag{14}$$

and the distribution of nuclei observed in simulations describes the form of $\Delta G_T(r)$ but not the amplitude. Nuclei are assumed to be spherical for $r > 2$ Å, which is proven to be valid in our previous studies [31, 33] and also observed in these simulations, meaning that the form of the free energy barrier can be represented by

$$\Delta G_T(r) = 4/3\pi r^3 A + 4\pi r^2 B, \tag{15}$$

where A and B are variables at each T and r_c can be estimated via $r_c = -2B/A$, equivalent to Eq. 11. If repeated for a range of T (and therefore δT) $r_c(T)$ is obtained. The free parameters γ, h_f and h_c are then found by fitting for $r_c(T)$ through

$$r_c(T) = \frac{-2\gamma}{h_f \frac{\delta T}{T_m}(1 - h_c \delta T)}, \tag{16}$$

where the h_f is the enthalpy of fusion and h_c accounts for non-linearity with temperature when defining the free energy liberated by freezing supercooled liquid

$$g^{sl} = h_f \frac{\delta T}{T} \left(1 - h_c \delta T\right). \tag{17}$$

Acknowledgements

We acknowledge a Natural Environment Research Council (NERC) grant, reference NE/T000228/1, which supports all authors on this project. AJW and CD acknowledge support from the NERC grant NE/V010867/1. AMW and CD acknowledge support from the NERC grant NE/T004835/1. DA acknowledges support from the NERC grants NE/M000990/1 and NE/R000425/1. For the purpose of Open Access, the author has applied a CC BY public copyright licence to any Author Accepted Manuscript (AAM) version arising from this submission.

Competing interests

The authors declare no competing interests.

Data availability

Original data underlying the analysis in this study is available at the repository doi.org/10.5281/zenodo.15310896.

Code availability

The LAMMPS (Large-scale Atomic/Molecular Massively Parallel Simulator) package is provided freely at https://lammps.sandia.gov/. Code used for analysis in this study is provided in the zenodo repository alongside data and is otherwise freely available.

Author contributions

A.J.W, C.J.D, A.M.W and D.A jointly conceived of the study, A.J.W performed research and analysis and A.J.W, C.J.D and A.M.W co-wrote the paper.

Correspondence and requests for materials should

be addressed to Alfred J. Wilson.

References

[1] Nimmo, F.: Thermal and compositional evolution of the core. Treatise on Geophysics **9**, 201–219 (2015)

[2] Davies, C.: Cooling history of earth's core with high thermal conductivity. Physics of the Earth and Planetary Interiors **247**, 65–79 (2015)

[3] Labrosse, S.: Thermal evolution of the core with a high thermal conductivity. Physics of the Earth and Planetary Interiors **247**, 36–55 (2015)

[4] Tarduno, J.A., Cottrell, R.D., Watkeys, M.K., Hofmann, A., Doubrovine, P.V., Mamajek, E.E., Liu, D., Sibeck, D.G., Neukirch, L.P., Usui, Y.: Geodynamo, solar wind, and magnetopause 3.4 to 3.45 billion years ago. science **327**(5970), 1238–1240 (2010)

[5] Fu, R.R., Drabon, N., Wiedenbeck, M., Brenner, A.R., Lowe, D.R., Borlina, C.S.: Paleomagnetism of 3.5-4.0 ga zircons from the barberton greenstone belt, south africa. Earth and Planetary Science Letters **567**, 116999 (2021)

[6] Bono, R.K., Paterson, G.A., Boon, A., Engbers, Y.A., Michael Grappone, J., Handford, B., Hawkins, L.M., Lloyd, S.J., Sprain, C.J., Thallner, D., *et al.*: The pint database: a definitive compilation of absolute palaeomagnetic intensity determinations since 4 billion years ago. Geophysical Journal International **229**(1), 522–545 (2022)

[7] Buffett, B.A., Huppert, H.E., Lister, J.R., Woods, A.W.: On the thermal evolution of the Earth's core. Journal of Geophysical Research: Solid Earth **101**(B4), 7989–8006 (1996)

[8] Gubbins, D., Alfè, D., Masters, G., Price, G.D., Gillan, M.: Gross thermodynamics of two-component core convection. Geophysical Journal International **157**(3), 1407–1414 (2004)

[9] Braginsky, S.: Structure of the f layer and reasons for convection in the earth's core. In: Soviet Phys. Dokl., vol. 149, pp. 8–10 (1963)

[10] Buffett, B.A., Seagle, C.T.: Stratification of the top of the core due to chemical interactions with the mantle. Journal of Geophysical Research: Solid Earth **115**(B4) (2010)

[11] Brodholt, J., Badro, J.: Composition of the low seismic velocity e′ layer at the top of earth's core. Geophysical Research Letters **44**(16), 8303–8310 (2017)

[12] Davies, C.J., Pozzo, M., Gubbins, D., Alfè, D.: Transfer of oxygen to Earth's core from a long-lived magma ocean. Earth and Planetary Science Letters **538**, 116208 (2020)

[13] Lay, T., Young, C.J.: The stably-stratified outermost core revisited. Geophysical Research Letters **17**(11), 2001–2004 (1990)

[14] Helffrich, G., Kaneshima, S.: Outer-core compositional stratification from observed core wave speed profiles. Nature **468**(7325), 807–810 (2010)

[15] Kaneshima, S.: Array analyses of smks waves and the stratification of earth's outermost core. Physics of the Earth and Planetary Interiors **276**, 234–246 (2018)

[16] Hirose, K., Wood, B., Vočadlo, L.: Light elements in the earth's core. Nature Reviews Earth & Environment **2**(9), 645–658 (2021)

[17] McDonough, W.F., Sun, S.-S.: The composition of the earth. Chemical geology **120**(3-4), 223–253 (1995)

[18] Birch, F.: Density and composition of mantle and core. Journal of geophysical research **69**(20), 4377–4388 (1964)

[19] McDonough, W.: 3.16–compositional model for the earth's core. Treatise on geochemistry, 559–577 (2014)

[20] Dauphas, N., Poitrasson, F., Burkhardt, C., Kobayashi, H., Kurosawa, K.: Planetary and meteoritic mg/si and δ30si variations inherited from solar nebula chemistry. Earth and Planetary Science Letters **427**, 236–248 (2015)

[21] Fischer, R.A., Nakajima, Y., Campbell, A.J., Frost, D.J., Harries, D., Langenhorst, F., Miyajima, N., Pollok, K., Rubie, D.C.: High pressure metal–silicate partitioning of Ni, Co, V, Cr, Si, and O. Geochimica et Cosmochimica Acta **167**, 177–194 (2015)

[22] Rubie, D.C., Jacobson, S.A., Morbidelli, A., O'Brien, D.P., Young, E.D., Vries, J., Nimmo, F., Palme, H., Frost, D.J.: Accretion and differentiation of the terrestrial

planets with implications for the compositions of early-formed solar system bodies and accretion of water. Icarus **248**, 89–108 (2015)

[23] Siebert, J., Badro, J., Antonangeli, D., Ryerson, F.J.: Terrestrial accretion under oxidizing conditions. Science **339**(6124), 1194–1197 (2013)

[24] Fischer, R.A., Campbell, A.J., Ciesla, F.J.: Sensitivities of Earth's core and mantle compositions to accretion and differentiation processes. Earth and Planetary Science Letters **458**, 252–262 (2017)

[25] Dziewonski, A.M., Anderson, D.L.: Preliminary reference earth model. Physics of the earth and planetary interiors **25**(4), 297–356 (1981)

[26] Badro, J., Côté, A.S., Brodholt, J.P.: A seismologically consistent compositional model of Earth's core. Proceedings of the National Academy of Sciences **111**(21), 7542–7545 (2014)

[27] Nimmo, F.: Energetics of the core. In: Schubert, G. (ed.) Treatise on Geophysics 2nd Edn vol. 8, pp. 27–55. Elsevier, Amsterdam (2015)

[28] Christian, J.W.: The Theory of Transformations in Metals and Alloys. Newnes, Boston (2002)

[29] Huguet, L., Van Orman, J.A., Hauck II, S.A., Willard, M.A.: Earth's inner core nucleation paradox. Earth and Planetary Science Letters **487**, 9–20 (2018)

[30] Davies, C., Pozzo, M., Alfè, D.: Assessing the inner core nucleation paradox with atomic-scale simulations. Earth and Planetary Science Letters **507**, 1–9 (2019)

[31] Wilson, A.J., Walker, A.M., Alfè, D., Davies, C.J.: Probing the nucleation of iron in earth's core using molecular dynamics simulations of supercooled liquids. Physical Review B **103**(21), 214113 (2021)

[32] Sun, Y., Zhang, F., Mendelev, M.I., Wentzcovitch, R.M., Ho, K.-M.: Two-step nucleation of the earth's inner core. Proceedings of the National Academy of Sciences **119**(2), 2113059119 (2022)

[33] Wilson, A.J., Alfè, D., Walker, A.M., Davies, C.J.: Can homogeneous nucleation resolve the inner core nucleation paradox? Earth and Planetary Science Letters **614**, 118176 (2023)

[34] Wilson, A., Davies, C., Walker, A., Alfe, D., Pozzo, M., Deuss, A.: Accepted: The formation and evolution of earth's inner core. Nature Reviews Earth & Environment **TBC**(TBC), (2025)

[35] Alfè, D., Gillan, M., Price, G.: Complementary approaches to the ab initio calculation of melting properties. The Journal of chemical physics **116**(14), 6170–6177 (2002)

[36] Wood, B.J.: Carbon in the core. Earth and Planetary Science Letters **117**(3-4), 593–607 (1993)

[37] Davies, C., Pozzo, M., Gubbins, D., Alfè, D.: Constraints from material properties on the dynamics and evolution of Earth's core. Nature Geoscience **8**(9), 678–685 (2015)

[38] Umemoto, K., Hirose, K.: Chemical compositions of the outer core examined by first principles calculations. Earth and Planetary Science Letters **531**, 116009 (2020)

[39] Ichikawa, H., Tsuchiya, T., Tange, Y.: The p-v-t equation of state and thermodynamic properties of liquid iron. Journal of Geophysical Research: Solid Earth **119**(1), 240–252 (2014)

[40] Andrault, D., Bolfan-Casanova, N., Nigro, G.L., Bouhifd, M.A., Garbarino, G., Mezouar, M.: Solidus and liquidus profiles of chondritic mantle: Implication for melting of the earth across its history. Earth and planetary science letters **304**(1-2), 251–259 (2011)

[41] Nomura, R., Hirose, K., Uesugi, K., Ohishi, Y., Tsuchiyama, A., Miyake, A., Ueno, Y.: Low core-mantle boundary temperature inferred from the solidus of pyrolite. Science **343**(6170), 522–525 (2014)

[42] Wahl, S.M., Militzer, B.: High-temperature miscibility of iron and rock during terrestrial planet formation. Earth and Planetary Science Letters **410**, 25–33 (2015)

[43] Takafuji, N., Hirose, K., Mitome, M., Bando, Y.: Solubilities of o and si in liquid iron in equilibrium with (mg, fe) sio3 perovskite and the light elements in the core. Geophysical Research Letters **32**(6) (2005)

[44] Alfè, D., Gillan, M., Price, G.D.: Composition and temperature of the Earth's core constrained by combining ab initio calculations and seismic data. Earth and Planetary Science Letters **195**(1-2), 91–98 (2002)

[45] Hirose, K., Labrosse, S., Hernlund, J.: Composition and state of the core. Annual Review of Earth and Planetary Sciences **41**(1), 657–691 (2013)

[46] Li, Y., Vočadlo, L., Alfè, D., Brodholt, J.: Carbon partitioning between the Earth's inner and outer core. Journal of Geophysical Research: Solid Earth **124**(12), 12812–12824 (2019)

[47] Masters, G., Gubbins, D.: On the resolution of density within the earth. Physics of the Earth and Planetary Interiors **140**(1-3), 159–167 (2003)

[48] Yuan, L., Steinle-Neumann, G.: Hydrogen distribution between the earth's inner and outer core. Earth and Planetary Science Letters **609**, 118084 (2023)

[49] Fischer, R.A., Cottrell, E., Hauri, E., Lee, K.K., Le Voyer, M.: The carbon content of earth and its core. Proceedings of the National Academy of Sciences **117**(16), 8743–8749 (2020)

[50] Blanchard, I., Rubie, D.C., Jennings, E.S., Franchi, I.A., Zhao, X., Petitgirard, S., Miyajima, N., Jacobson, S.A., Morbidelli, A.: The metal–silicate partitioning of carbon during earth's accretion and its distribution in the early solar system. Earth and Planetary Science Letters **580**, 117374 (2022)

[51] Côté, A.S., Vočadlo, L., Brodholt, J.P.: The effect of silicon impurities on the phase diagram of iron and possible implications for the earth's core structure. Journal of Physics and Chemistry of Solids **69**(9), 2177–2181 (2008)

[52] Badro, J., Brodholt, J.P., Piet, H., Siebert, J., Ryerson, F.J.: Core formation and core composition from coupled geochemical and geophysical constraints. Proceedings of the National Academy of Sciences **112**(40), 12310–12314 (2015)

[53] Lasbleis, M., Kervazo, M., Choblet, G.: The fate of liquids trapped during the earth's inner core growth. Geophysical Research Letters **47**(2), 2019–085654 (2020)

[54] Pang, G., Koper, K.D., Wu, S.-M., Wang, W., Lasbleis, M., Euler, G.: Enhanced inner core fine-scale heterogeneity towards earth's centre. Nature **620**(7974), 570–575 (2023)

[55] Driscoll, P., Davies, C.: The "new core paradox:" challenges and potential solutions. Journal of Geophysical Research: Solid Earth, 2022–025355 (2023)

[56] Biggin, A.J., Piispa, E., Pesonen, L.J., Holme, R., Paterson, G., Veikkolainen, T., Tauxe, L.: Palaeomagnetic field intensity variations suggest mesoproterozoic inner-core nucleation. Nature **526**(7572), 245–248 (2015)

[57] Bono, R.K., Tarduno, J.A., Nimmo, F., Cottrell, R.D.: Young inner core inferred from ediacaran ultra-low geomagnetic field intensity. Nature Geoscience **12**(2), 143–147 (2019)

[58] Badro, J., Aubert, J., Hirose, K., Nomura, R., Blanchard, I., Borensztajn, S., Siebert, J.: Magnesium partitioning between Earth's mantle and core and its potential to drive an early exsolution geodynamo. Geophysical Research Letters **45**(24), 13–240 (2018)

[59] Hirose, K., Morard, G., Sinmyo, R., Umemoto, K., Hernlund, J., Helffrich, G., Labrosse, S.: Crystallization of silicon dioxide and compositional evolution of the Earth's core. Nature **543**(7643), 99–102 (2017)

[60] Wilson, A.J., Pozzo, M., Alfè, D., Walker, A.M., Greenwood, S., Pommier, A., Davies, C.J.: Powering earth's ancient dynamo with silicon precipitation. Geophysical Research Letters **49**(22), 2022–100692 (2022)

[61] Wilson, A.J., Pozzo, M., Davies, C.J., Walker, A.M., Alfè, D.: Examining the power supplied to earth's dynamo by magnesium precipitation and radiogenic heat production. Physics of the Earth and Planetary Interiors **343**, 107073 (2023)

[62] Mittal, T., Knezek, N., Arveson, S.M., McGuire, C.P., Williams, C.D., Jones, T.D., Li, J.: Precipitation of multiple light elements to power Earth's early dynamo. Earth and Planetary Science Letters **532**, 116030 (2020)

[63] Kresse, G., Furthmüller, J.: Efficient iterative schemes for ab initio total-energy calculations using a plane-wave basis set. Physical review B **54**(16), 11169 (1996)

598 [64] Kresse, G., Joubert, D.: From ultrasoft pseudopotentials to the projector
599 augmented-wave method. Physical review b **59**(3), 1758 (1999)

600 [65] Perdew, J.P., Chevary, J.A., Vosko, S.H., Jackson, K.A., Pederson, M.R., Singh,
601 D.J., Fiolhais, C.: Atoms, molecules, solids, and surfaces: Applications of the
602 generalized gradient approximation for exchange and correlation. Physical review
603 B **46**(11), 6671 (1992)

604 [66] Plimpton, S.: Fast parallel algorithms for short-range molecular dynamics.
605 Journal of computational physics **117**(1), 1–19 (1995)

606 [67] Wolde, P., Ruiz-Montero, M.J., Frenkel, D.: Numerical calculation of the rate
607 of crystal nucleation in a lennard-jones system at moderate undercooling. The
608 Journal of chemical physics **104**(24), 9932–9947 (1996)